OPEN

Can Ex Vivo Magnetic Resonance Imaging of Rectal Cancer Specimens Improve the Mesorectal Lymph Node Yield for Pathological Examination?

Rutger Stijns, MD,† Bart Philips, MD,* Carla Wauters, MD, PhD,‡ Johannes de Wilt, MD, PhD,† Iris Nagtegaal, MD, PhD,§ and Tom Scheenen, PhD**

Purpose: The aim of this study was to use 7 T ex vivo magnetic resonance imaging (MRI) scans to determine the size of lymph nodes (LNs) in total mesorectal excision (TME) specimens and to increase the pathological yield of LNs with MR-guided pathology.

Materials and Methods: Twenty-two fixated TME specimens containing adenocarcinoma were scanned on a 7 T preclinical MRI system with a T1-weighted 3-dimensional gradient echo sequence with frequency-selective lipid excitation (repetition time/echo time, 15/3 milliseconds; resolution, 0.293 mm^3) and a water-excited 3-dimensional multigradient echo (repetition time, 30 milliseconds; computed echo time, 6.2 milliseconds; resolution, 0.293 mm^3) pulse sequence.

The first series of 11 TME specimens (S1) revealed the number and size of LNs on both ex vivo MRI and histopathology. The second series of 11 TME specimens (S2) was used to perform MR-guided pathology. The number, size, and percentages of yielded LNs of S1 and S2 were compared.

Results: In all specimens (22/22), a median number of 34 LNs (interquartile range, 26–34) was revealed on ex vivo MRI compared with 14 LNs (interquartile range, 7.5–21.5) on histopathology ($P = 0.003$). Mean size of all LNs did not differ between the 2 series (ex vivo MRI: 2.4 vs 2.5 mm, $P = 0.267$; pathology: 3.6 vs 3.5 mm, $P = 0.653$). The median percentages of harvested LNs compared with nodes visible on ex vivo MRI per specimen for both series were not significantly different (40% vs 43%, $P = 0.718$). By using a size threshold of greater than 2 mm, the percentage improved to 71% (S1) and to 78% (S2, $P = 0.895$). The median number of harvested LNs per specimen did not increase by performing MR-guided pathology (S1, 14 LNs; S2, 20 LNs; $P = 0.532$).

Conclusions: Ex vivo MRI visualizes more LNs than (MR-guided) pathology is able to harvest. Current pathological examination was not further improved by MR guidance. The majority of LNs or LN-like structures visible on ex vivo MRI below 2 mm in size remain unexplained, which warrants a 3-dimensional approach for pathological reconstruction of specimens.

Key Words: rectal cancer, magnetic resonance imaging, lymph node, pathology, yield

(*Invest Radiol* 2019;54: 645–652)

The presence of lymph node (LN) metastases determines the treatment regimen in rectal cancer patients. Magnetic resonance imaging (MRI) is known to be the superior 3-dimensional imaging modality to identify and characterize the tumor as well as LNs in vivo with a high spatial resolution.[1] T2-weighed fast-spin echo sequences in particular enable detailed visualization of the anatomy of the pelvis. Lymph nodes that are likely to be involved in rectal cancer are located in the mesorectum. The fatty tissue surrounding the rectum with an outer border defined as the mesorectal fascia, which forms an important anatomical barrier for tumor spread. Metastatic LNs are a strong risk factor for local recurrence and for (disease-free) survival, also after curative treatment.[2] The cornerstone of curative treatment of the disease is resection according to the principle of a total mesorectal excision (TME).[3] Neoaduvant (chemo)radiotherapy is given before surgery in case of suspected LN metastases or in case of locally advanced disease on clinical MRI.[4]

The approach for surgical resection in TME surgery depends on the height of the lower pole of the tumor to the anorectal junction.[5] Proximal or middle rectal tumors are treated with an anterior resection and distal rectal tumors with an abdominoperineal excision.[6–10] Both approaches have significant morbidity and can result in an impaired quality of life.[11,12] The current clinical histopathological evaluation of TME specimens focuses on tumor staging according to the TNM criteria of the American Joint Cancer Committee.[4,13] Next to assessing the extent of the primary tumor, LNs are detected by inspection and palpation of thin axial tissue slices. International guidelines prescribe a minimum pathological yield of 12 LNs.[14–16] National guidelines may deviate from this, such as in the Netherlands where 10 evaluated LNs are considered to be sufficient.[17] There are many factors that can influence LN yield such as age, surgery, systemic diseases, and preoperative treatment.[18,19] Especially preoperative treatment in the form of (chemo)radiotherapy can lead to a reduced LN yield potentially leading to understaging.[18,20] High-quality pathological assessment of a TME specimen is therefore crucial.

Multiple studies have aimed to improve LN yield of pathological evaluation investigating LN markers, such as methylene blue staining.[21–24] Until now, no research focused on the use of ex vivo MRI to visualize LNs in a TME specimen. Clinical MR systems for in vivo staging of the disease normally have a magnetic field-strength of 1.5 or 3 T. Surgical specimens can be examined with preclinical MR systems with a smaller magnet bore size, higher magnetic field strength, and stronger magnetic field gradients. By applying dedicated ex vivo MRI to rectal specimens, 3-dimensional imaging at a high spatial resolution can be obtained with visualization of all LNs present in a rectal specimen.[25] Subsequently, these images can be used to guide the pathologist toward the visible LNs during pathological workup.

Received for publication January 29, 2019; and accepted for publication, after revision, April 15, 2019.

From the Departments of *Radiology and Nuclear Medicine, and †Surgery, Radboud University Medical Centre; ‡Department of Pathology, Canisius-Wilhelmina Hospital; and §Department of Pathology, Radboud University Medical Centre, Nijmegen, the Netherlands.

Conflicts of interest and sources of funding: Authors declare no conflicts of interest. This work was supported by the Department of Radiology and Nuclear Medicine at the Radboud University Medical Center.

Supplemental digital contents are available for this article. Direct URL citations appear in the printed text and are provided in the HTML and PDF versions of this article on the journal's Web site (www.investigativeradiology.com).

Correspondence to: Rutger Stijns, MD, Department of Radiology and Nuclear Medicine, Radboud University Medical Centre, Route 767, Geert Grooteplein Zuid 10, 6525-GA Nijmegen, the Netherlands. E-mail: Rutger.Stijns@Radboudumc.nl.

ISSN: 0020-9996/19/5410–0645
DOI: 10.1097/RLI.0000000000000581

In this study, we developed a protocol for the use of 7 T ex vivo MRI scans of TME specimens to determine the number and size of mesorectal LNs thereby aiming to increase the pathological LN harvest after MR-guided pathology.

METHODS

Design and Eligibility

A prospective, observational study to evaluate 2 series of rectal cancer specimens was conducted in 2 referral centers for rectal cancer treatment. The first series of rectal specimens (S1) was examined to establish the number and size of LNs separately on ex vivo MRI and on standard histopathology. Histopathology of the first series was performed in a standard workup with normal duration by pathologists unaware of this study. Lymph nodes detected on ex vivo MRI of the second series (S2) were used to guide the pathologist during pathologic examination of the specimen. Pathological workup for S2 was an extensive search with a maximum of 2 hours. The number, size, and percentages of yielded LNs of S1 and S2 were then compared. The number of LNs visible on clinical in vivo T2-weighted MRI scans was also assessed (repetition time [TR] and echo time [TE] of 3680–4980 milliseconds and 93–95 milliseconds; resolution, $0.5 \times 0.5 \times 3.0$ mm^3). The study design is illustrated in Supplemental Figure 1, Supplemental Digital Content 1, http://links.lww.com/RLI/A440. This study was approved by the institutional review board of the medical ethical research committee of the Radboud University Medical Centre with a waiver of informed consent (registration number 2016–2490).

Patients

Twenty-two surgical specimens from patients with biopsy-proven rectal cancer who were treated with a total mesenteric excision were included in the study. The admission of neoadjuvant treatment according to Dutch clinical guidelines—short-course radiotherapy or long-course chemoradiotherapy—was no exclusion criterion.

Ex Vivo Magnetic Resonance Imaging

Magnetic resonance imaging of fixated rectal cancer specimens was performed on a horizontal 7 T preclinical MR system (ClinScan; Bruker BioSpin, Ettlingen, Germany) using a volume coil. Next to a localizer, the MR protocol consisted of 2 parts: one part focused on imaging lipids, and the other part focusing on imaging of water, similar to in vivo MRI of LNs at ultrahigh field strength.[26] Magnetic resonance imaging of lipids was performed with a T1-weighted 3-dimensional gradient echo (GRE) sequence with frequency-selective lipid excitation at a high isotropic spatial resolution of $0.29 \times 0.29 \times 0.29$ mm^3 TR and TE of 15 and 3 milliseconds, and excitation flip angle of 10 degrees. Magnetic resonance imaging of water consisted of a 3-dimensional multi-GRE pulse sequence of 5 acquired echoes and frequency-selective water excitation at the same spatial resolution (TR, 30 milliseconds; multiple TEs of 3.0, 7.6, 12.1, 16.6, 21.2 milliseconds, combined into one computed TE image of 6.2 milliseconds; excitation flip angle of 14 degrees).[26] All TME specimens were of a size larger than 10 cm and were scanned in multiple sections. These were merged to one composed lipid and one inherently coregistered water 3-dimensional MR image dataset.

To evaluate the ex vivo MR images, annotations were drawn around the LNs on composed lipid and water-selective GRE images. Two datasets were used simultaneously in search of spherical structures suggested to be an LN. An LN, or an LN-like structure, was defined as a spherical structure visible in 3 dimensions with low signal intensity on lipid and high signal intensity on water-selective GRE images, respectively. The assessment and differentiation between small blood vessels and LNs was performed by simultaneously evaluating transverse, sagittal, and coronal cross-sections through the datasets. All ex vivo MR images were evaluated by a trained researcher to assess the number and size of LNs or LN-like structures present in the TME specimen. The reader was able to make thin maximum intensity projections.

MR-Guided Pathology

Lymph nodes detectable on ex vivo MRI of S2 were annotated using the software package MeVisLab (MeVis Medical Solutions,

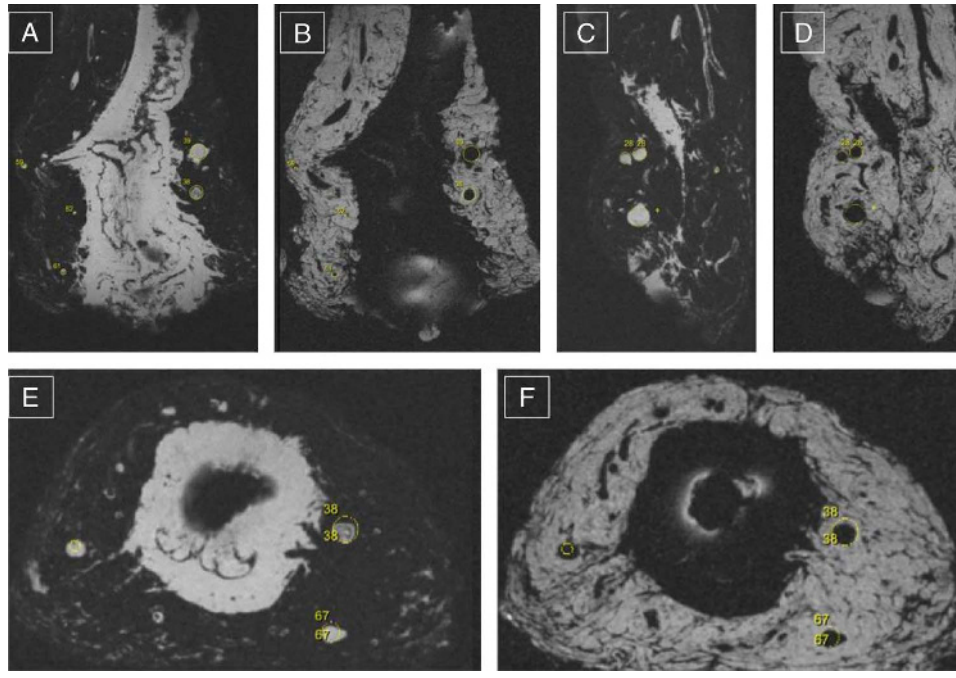

FIGURE 1. Example of a 3-dimensional dataset (A, coronal plane; B, sagittal plane; C and D, axial plane) of water- and lipid- (left, right) selective imaging that was used to guide the pathologist toward structures as annotated with the yellow circles and numbers in the different images.

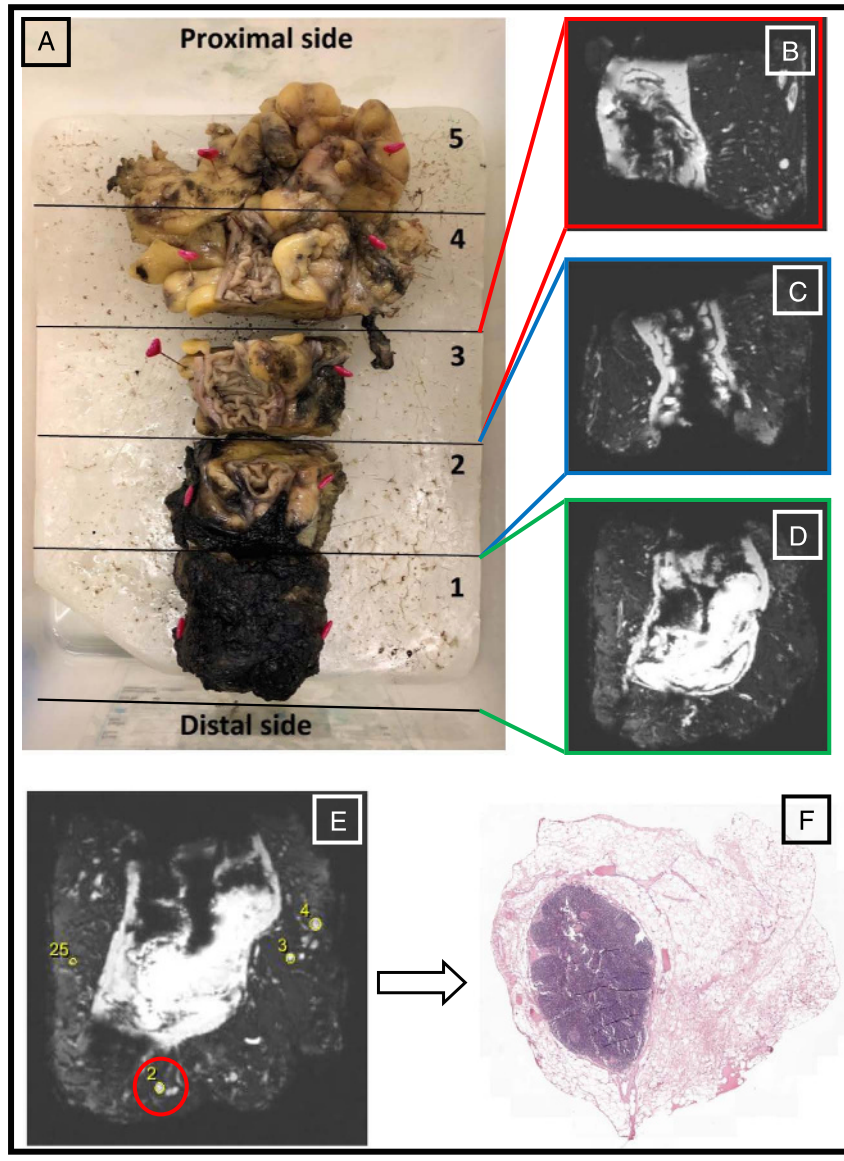

FIGURE 2. Rectal specimen (A) that was examined using MR-guided pathology to harvest the smallest lymph nodes. In this specimen, separate tissue samples were scanned individually and used for guidance (B–D). A small lymph node of 2 mm on MRI (E, red circle) and on pathology (F) was detected with this specific MR-guided pathology approach.

Fraunhofer MEVIS). The annotations were shown to the pathologist during the macroscopic specimen examination. The trained researcher who evaluated the ex vivo MR images was present during the specimen examination and provided a laptop with MR datasets with annotated structures to provide navigation during pathology. Every spherical structure in 3 dimensions detected on MRI was supposed to be harvested. The pathologist and trained researcher used the MR images and annotations together to locate and yield LN-like structures present in the surgical specimen. Conventional pathological examination (S1) took approximately 30 minutes per specimen to stage the primary tumor and harvest the LNs. A timeslot of 120 minutes was reserved for MR-guided pathological evaluation (S2) per TME specimen.

Histopathological Preparation and Diagnosis

All specimens were fixated in 10% buffered formalin for at least 48 hours before ex vivo MRI. Macroscopic evaluation was done by slicing the specimen from the distal resection margin to the proximal margin in serial transverse tissue lamina at a 5-mm interval. Each transverse tissue slice was evaluated by inspection, palpation, and perpendicular slicing. Detected LNs or fatty tissue thought to contain LNs were then embedded in paraffin. Subsequently, sections of 4-μm thickness were sliced from each embedded paraffin tissue block, mounted on glass slides (6 × 2 cm), and stained with hematoxylin-eosin. In case of absence of LNs during microscopy, multiple cross-sections of the paraffin-embedded tissue block were prepared to verify the presence of LNs. In addition, D2-40 and CD34 immunohistochemistry was performed on a selection of fragments to expose lymphatic and/or vascular structures.[27]

Statistical Analysis

The LN harvest by using MR-guided pathology compared with standard pathologic workup was evaluated. Baseline characteristics of the included patients were compared using the unpaired t test. The median number of LNs examined in both series was calculated for explanatory variables across all stages. The number, size, and percentages of

detected LNs of the 2 series were compared. T tests, χ^2 tests, and Mann-Whitney *U* tests were used to determine the statistical significance of differences for ordinal and categorical variables, respectively. A *P* value of less than 0.05 was considered to be statistically significant. The data were analyzed with the SPSS Statistics V22.0 (SPSS Inc, Chicago, IL). Sizes and frequencies were additionally displayed in histograms made with Graphpad Prism 5.03 (GraphPad Software, Inc).

RESULTS

Twenty-two TME specimens with biopsy-proven adenocarcinoma of the rectum were included in the study. All 22 specimens were successfully scanned with our protocol designed for ex vivo 7 T lipid and water-selective MRI. The composed lipid and water-selective datasets were used for the detection of round-shaped structures, and all structures visible could be evaluated in 3 dimensions. An example of the 3-dimensional MR datasets is displayed in Figures 1 and 2. Relevant patient-related baseline and pathology characteristics did not reveal significant differences, except for the mean age (Table 1).

In general, more LN-like structures were discovered on MRI than LNs were harvested during pathological examination. On clinical in vivo MR images, a median number of 14 LNs for S1 (interquartile range [IQR], 8–16) and 12 LNs for S2 (IQR, 8–16) were visible, without statistical significant difference ($P = 0.899$). Overall, a median number of 34 (IQR, 26–43) and 14 (IQR, 7.5—21.5) LNs per specimen were revealed on ex vivo MRI and histopathology, respectively. This median difference in yield was significant for both series (S1, $P = 0.003$; S2, $P = 0.004$, calculated with Mann-Whitney *U* test). For each individual specimen, the total number of LNs or LN-like structures that was detected on ex vivo MRI was the largest over in vivo or histopathologically detected nodes (Fig. 3, A and B). Numbers and size for detected LNs on ex vivo MRI and during pathological examination for both series are presented in Table 2. The mean size of all LNs did not differ between the 2 series (ex vivo MRI: 2.4 mm vs 2.5 mm, $P = 0.267$; pathology: 3.6 mm vs 3.5 mm, $P = 0.653$; calculated with 1-sample t test). The admission of neoadjuvant chemoradiotherapy did not lead to a mean size difference between harvested LNs. The size distribution of harvested LNs appeared similar between the 2 series (Fig. 4). Final pathological assessment showed no differences between both series for the median number of LNs harvested during pathological examination (14 LNs for S1, range 4–30; and 20 LNs for S2, range 5–29; $P = 0.532$).

Ratios of LN yield compared with the number of LNs detected on ex vivo MRI were calculated to provide further insight in the potential benefit of MR-guided pathology. A median 40% (range, 13%–95%) of the nodes visible on ex vivo MRI were pathologically harvested for S1 and 43% (range, 27%–73%) for S2. By using a size threshold for nodes larger than 2 mm, the median percentage of harvested LNs improved to 71% (range, 20%–150%) and 78% (range, 38%–250%) for S1 and S2, respectively. Statistical significance was tested by using the Mann-Whitney *U* test.

The paraffin-embedded tissue blocks of 34 tissue fragments in which initially no LNs were found were cross-sectioned multiple times. This subanalysis revealed 2 additional LNs (an example is illustrated in Supplemental Fig. 2, Supplemental Digital Content 2, http://links.lww.com/RLI/A441). The cross-sections of the 32 other tissue blocks revealed nerve branches and blood vessels. The D2-40 and CD34 immunohistochemistry was also performed on these tissue samples. The immunohistochemical analysis using D2-40 and CD34 did not expose any additional lymphatic structures in these fragments.

DISCUSSION

In this work, we evaluated the use of ultrahigh field MRI of surgical TME specimens to guide pathology for extensive LN staging. Our MR protocol enabled obtaining isotropic, high spatial resolution images of good quality. This 3-dimensional MR visualization of a surgical specimen is, to

TABLE 1. Baseline Characteristics and Findings for Standard and Magnetic Resonance–Guided Pathology for Patients Assigned to S1 or S2

	Series 1 (n = 11)	Series 2 (n = 11)	*P*
Mean age, y	62	68	0.024 (t test)
Sex			
Male	5	9	0.076 (χ^2)
Female	6	2	
Neoadjuvant treatment			
None	5	6	0.540 (χ^2)
Short-course radiotherapy	3	1	
Chemoradiotherapy	3	4	
Surgery			
Low anterior resection	8	5	0.193 (χ^2)
Abdominoperieal excision	3	6	
Pathological T stage			
pT0	1	2	0.316 (χ^2)
pT1	1	4	
pT2	3	1	
pT3	6	4	
pT4	0	0	
Pathological N stage			
pN0	6	8	0.319 (χ^2)
pN1	3	3	
pN2	2	0	
Malignant nodes (median)	1.0 (0–7)	0.0 (0–2)	0.284 (Mann-Whitney *U* test)
Total nodes (median)	14.0 (4–30)	20.0 (5–29)	0.532 (Mann-Whitney *U* test)

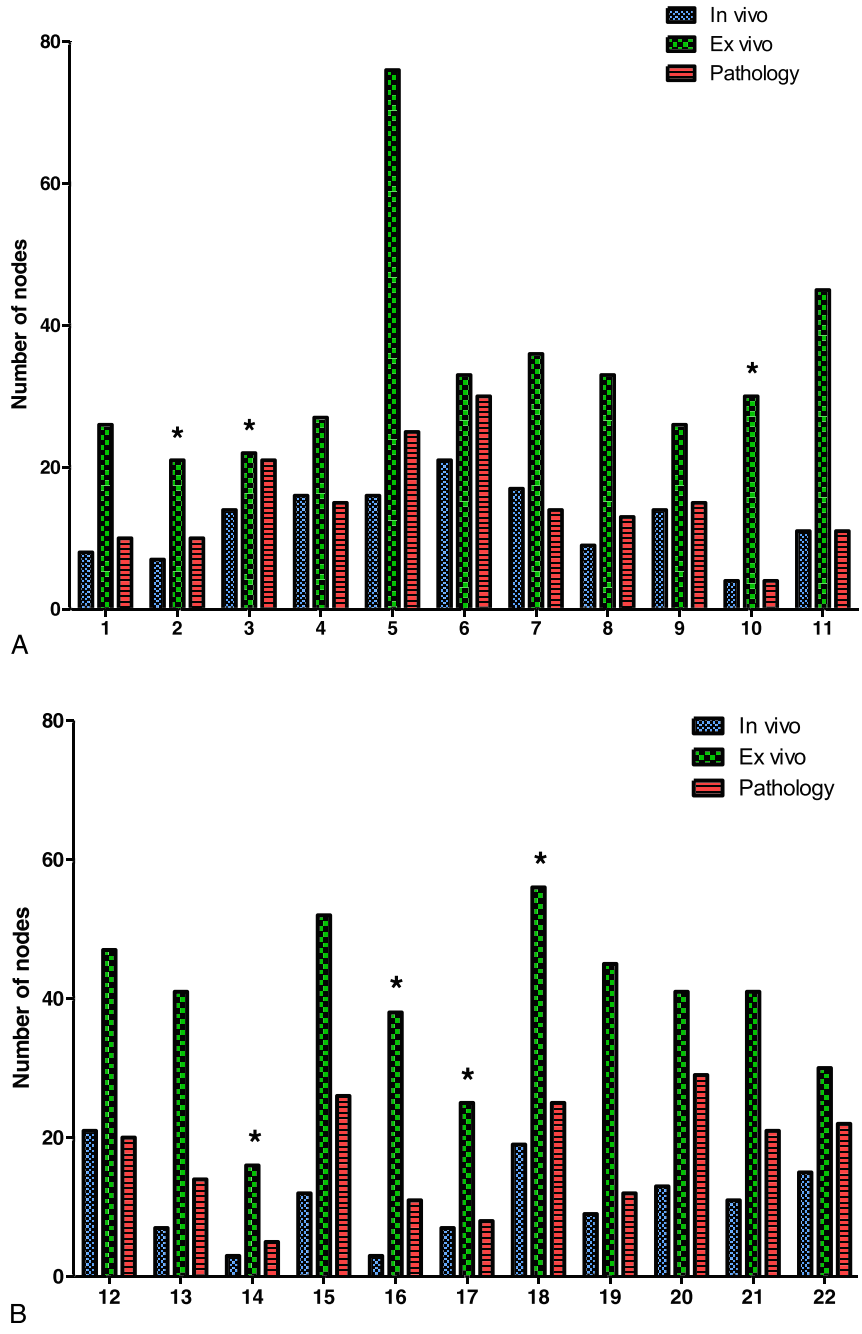

FIGURE 3. Number of lymph nodes per specimen found on in vivo and ex vivo MRI and pathology for (A) series 1 and for (B) series 2. Asterisk marks patients treated with neoadjuvant chemoradiotherapy.

our knowledge, a novel approach to interpret and use ex vivo ultrahigh field MRI for pathological support. By performing lipid and water-selective imaging on a specimen that consists of a substantial proportion of lipid tissue, LNs, and blood vessels, recognition of LNs or small water-containing spherical structures could be done in a straightforward way.

Unfortunately, the current study did not show an effect of MR guidance on the number and size of LN harvested from a rectal specimen. A remarkable finding was that ex vivo MRI visualized significantly more and significantly smaller LNs than those yielded during pathological examination. Even with additional effort consisting of multiple sectioning and immunohistochemistry of excised tissue fragments, an increased pathological LN yield could not be verified. No histological substrate was detected for small structures that were clearly visible on ex vivo MRI, which leaves us in nescience on the exact anatomy of these radiological structures. The hypothesis that these LN-like structures could be found using MR-guided pathology was not confirmed. The question arises what those less than 2 mm MR structures could be, apart from LNs. It could be that these structures are LNs, but are missed during pathological evaluation. If not seen or palpated, it is challenging to incorporate the correct corresponding tissue fragments for further histological workup. Moreover, in 4 patients, minor differences between the number of LNs on ex vivo MRI and pathology were seen, without any specimen- or scanning-specific explanation for this observation. These specimens did show a relatively large proportion

TABLE 2. Numbers and Size for Detected LNs on Ex Vivo MRI and During Pathological Examination for Both Series

	Series 1			Series 2			*P* of % LN Harvest
A. All lymph nodes together							
	Ex Vivo MRI (n = 11)	Pathology (n = 11)	Total % Harvested	Ex Vivo MRI (n = 11)	Pathology (n = 11)	Total % Harvested	
Total nodes	375	168	44.8%	432	193	44.7%	0.636
Mean size, mm	2.4 (0.7–8.0)	3.6 (0.5–10)		2.5 (0.5–8.9)	3.5 (1.0–13.0)		—
B, No preoperative treatment or short-course radiotherapy							
	Ex Vivo MRI (n = 8)	Pathology (n = 8)	% Harvested	Ex Vivo MRI (n = 7)	Pathology (n = 7)	% Harvested	
Total nodes	302	133	44%	267	122	52.2%	0.306
Mean size, mm	2.6 (0.7–8.0)	3.7 (0.5–10.0)		2.6 (0.1–6.2)	3.7 (1.0–13.0)		—
C. Preoperative chemoradiotherapy							
	Ex Vivo MRI (n = 3)	Pathology (n = 3)		Ex Vivo MRI (n = 4)	Pathology (n = 4)	% Harvested	
Total nodes	73	35	47.9%	135	49	36.3%	0.459
Mean size, mm	2.3 (0.8–4.1)	3.2 (1.0–8.0)		2.0 (1.1–5.1)	2.3 (1.0–5.0)		—

A, total number and size of lymph nodes detected on ex vivo MRI and pathology per series. B, number and size of lymph nodes from rectal specimens without preoperative treatment or with preoperative short-course radiotherapy. C, number and size of lymph nodes from rectal specimens with preoperative chemoradiotherapy.

*P values for differences in % LN harvest were calculated using t test.

LN indicates lymph node; MRI, magnetic resonance imaging.

of LNs larger than 2 mm on ex vivo MRI (59%–88%), which are theoretically easier to find during pathological evaluation.

Multiple microscopic cross-sections of tissue fragments not immediately revealing LNs that were visible on ex vivo MRI revealed vascular structures, nerve branches, or only lipid tissue on microscopic evaluation. On a simultaneous evaluation of transverse, sagittal, and coronal MR images, these representations of tubular structures such as vessels and nerves can be easily differentiated from the appearance of LNs. The 3-dimensional visualization with high spatial resolution makes it unlikely to mistake LNs for tubular structures. The application of MR-guided pathology can be suffering from a learning curve, as a result of which the effect of MR-controlled pathology is not yet visible. It seems plausible that the translation from a 3-dimensional MR dataset (Supplementary Fig. 3, Supplemental Digital Content 3, http://links.lww.com/RLI/A442) to a 2-dimensional approach such as current pathological evaluation is even more challenging than presumed, which might have resulted in missing LNs below a certain size. Perhaps, a 3-dimensional pathological approach of TME specimens may improve the anatomical correlation of 3-dimensional MRI with pathology.

Optimizing pathologic LN staging and LN yield has previously been investigated. Zhang et al[28] aimed to predict the presence of LN metastases by evaluating chemical shift effects on ex vivo images with promising results. Although the prediction of the LN status was not investigated in the current study, a combination of in vivo and ex vivo ultrahigh field MRI and LN prediction would be interesting.[26,29] Recent literature regarding pathological improvements mainly focused on the postoperative use of methylene blue staining.[21,22,24,30–33] Methylene blue injection into the superior rectal artery significantly increased the mean number of LN harvest in rectal cancer patients treated by TME surgery with and without neoadjuvant chemoradiotherapy. Also LN revealing solutions such as GEWF (glacial acetic acid, ethanol, water and formalin) and acetone have been investigated to enhance the total LN retrieval from rectal specimens.[34] Not only larger but also smaller LNs were retrieved using these solutions. However, not only the quantity of evidence is limited, but also usage of these solutions involves health risks for people working with these substances. Thus, although these pathology preparations identify the presence of more and smaller nodes, they are not widely integrated in standard pathological workup.

The accuracy for the prediction of involved mesorectal LNs using MRI in vivo is approximately 75% to 80%.[1] Morphological features such as irregular border, signal heterogeneity, and a round shape combined with size is the best predictor of nodal involvement, but is subject to interreader variability, and accuracy drops significantly for small LNs.[35] There is increasing evidence that small LNs (≤3 mm) can contain tumor metastases.[25] Wang et al[36] described a series of 31 rectal specimens that were examined for patterns of tumor spread and metastasis. One hundred twenty-eight of 972 examined LNs in this study contained tumor metastases, of which approximately 93% of the metastatic nodes were of a size 0.5 to 5 mm. Märkl et al[37] showed that in colon cancer, where neoadjuvant treatment has no role, LN metastases were discovered in nodes with a size of 1 to 5 mm. These results imply that the detection of small LNs in rectal cancer is also relevant to prevent pathological understaging, especially because neoadjuvant (chemo)radiotherapy is thought to further reduce the number and size of LNs.[18]

The mean number of LNs examined in literature varies from 14 to 20 nodes per specimen, which is in line with current international standards.[33,38–40] Variations between pathology laboratories are known regarding the number of LNs that are evaluated in rectal cancer. This variety may be dependent on the biology of the tumor, but is also related to the effort of the surgical and pathology team.[41,42] Academic and teaching hospitals with different resources and workload are thought to produce and examine a larger number of LNs.[43–45] The current study was performed in academic and/or teaching centers for rectal cancer treatment. This might explain why LN yield did not increase by the additional MR guidance. On the other hand, it can be stated that current standard pathologic

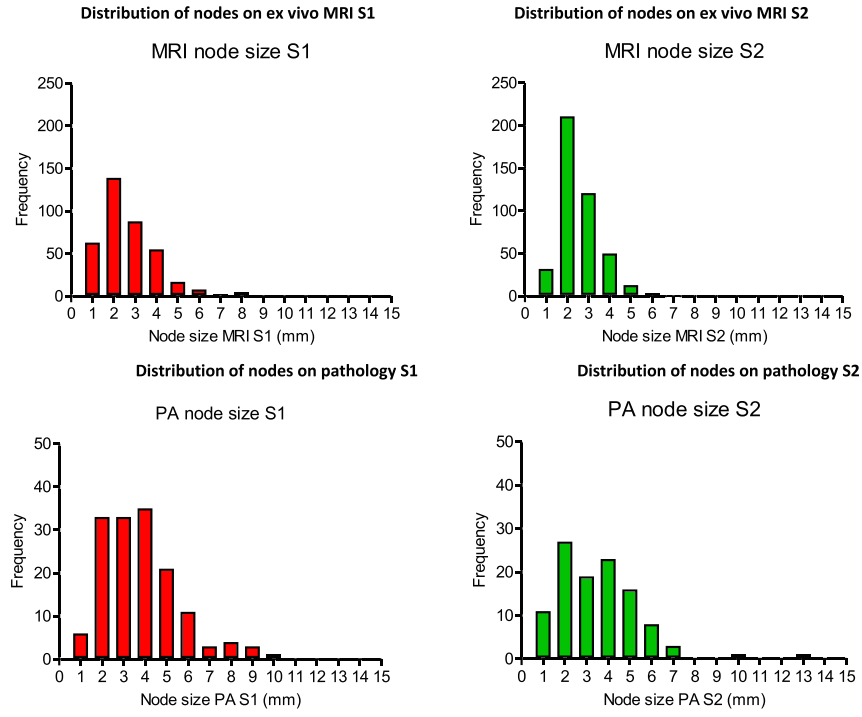

FIGURE 4. Size distribution of lymph nodes on ex vivo MRI and pathology.

examination is sufficient in harvesting the number of LNs as subscribed by international guidelines.[4]

This study has some limitations. First, the study cohort of 22 specimens may not be large enough to prove a significant difference in median LN harvest between the 2 approaches. Second, a large proportion of the ex vivo MRI annotated LNs could not be detected during pathology. Although we were able to obtain high-quality lipid and water-selective MRI, which enabled a more or less straightforward recognition of LN-like structures in 3 dimensions, the question whether all these structures are indeed LNs remained unanswered. A 3-dimensional pathological analysis of the whole specimens could provide further insight in future studies.

CONCLUSIONS

In conclusion, ex vivo 7 T MRI at a high spatial resolution visualized structures that were challenging to harvest during (MR-guided) pathology. The current study design with MR guidance was not able to further improve standard pathological workup to increase the LN yield. The histological origin of the majority of spherical structures below 2 mm in size on MRI remained unconfirmed, which warrants a 3-dimensional approach for pathological reconstruction of specimens.

REFERENCES

1. Al-Sukhni E, Milot L, Fruitman M, et al. Diagnostic accuracy of MRI for assessment of T category, lymph node metastases, and circumferential resection margin involvement in patients with rectal cancer: A systematic review and meta-analysis. *Ann Surg Oncol*. 2012;19:2212–2223.
2. Kapiteijn E, Marijnen CA, Nagtegaal ID, et al. Preoperative radiotherapy combined with total mesorectal excision for resectable rectal cancer. *N Engl J Med*. 2001;345:638–646.
3. Heald RJ, Ryall RD. Recurrence and survival after total mesorectal excision for rectal cancer. *Lancet*. 1986;1:1479–1482.
4. Glynne-Jones R, Wyrwicz L, Tiret E, et al. Rectal cancer: ESMO Clinical Practice Guidelines for diagnosis, treatment and follow-up. *Ann Oncol*. 2017;28(suppl 4): iv22–iv40.
5. Bujko K, Rutkowski A, Chang GJ, et al. Is the 1-cm rule of distal bowel resection margin in rectal cancer based on clinical evidence? A systematic review. *Ann Surg Oncol*. 2012;19:801–808.
6. Scott N, Jackson P, Al-Jaberi T, et al. Total mesorectal excision and local recurrence: a study of tumour spread in the mesorectum distal to rectal cancer. *Br J Surg*. 1995;82:1031–1033.
7. Nagtegaal ID, Knijn N, Hugen N, et al. Tumor deposits in colorectal cancer: improving the value of modern staging—a systematic review and meta-analysis. *J Clin Oncol*. 2017;35:1119–1127.
8. Nelson H, Petrelli N, Carlin A, et al. Guidelines 2000 for colon and rectal cancer surgery. *J Natl Cancer Inst*. 2001;93:583–596.
9. Law WL, Chu KW. Anterior resection for rectal cancer with mesorectal excision: a prospective evaluation of 622 patients. *Ann Surg*. 2004;240:260–268.
10. Glimelius B, Tiret E, Cervantes A, et al. Rectal cancer: ESMO Clinical Practice Guidelines for diagnosis, treatment and follow-up. *Ann Oncol*. 2013;24(suppl 6): vi81–vi88.
11. Thaysen HV, Jess P, Laurberg S. Health-related quality of life after surgery for primary advanced rectal cancer and recurrent rectal cancer: a review. *Colorectal Dis*. 2012;14:797–803.
12. Stijns RCH, Tromp MR, Hugen N, et al. Advances in organ preserving strategies in rectal cancer patients. *Eur J Surg Oncol*. 2018;44:209–219.
13. Weisenberg E. *TNM Staging of Colorectal Carcinoma, AJCC 8th Edition*.
14. Awwad GE, Tou SI, Rieger NA. Prognostic significance of lymph node yield after long-course preoperative radiotherapy in patients with rectal cancer: a systematic review. *Colorectal Dis*. 2013;15:394–403.
15. Sobin LH, Gospodarowicz MK, Wittekind C. *TNM Classification of Malignant Tumours*. 7th ed. Wiley-Blackwell; 2009.
16. Compton CC, Fielding LP, Burgart LJ, et al. Prognostic factors in colorectal cancer. College of American Pathologists Consensus Statement 1999. *Arch Pathol Lab Med*. 2000;124:979–994.
17. Tumoren LwGI. Colorectaalcarcinoom Landelijke richtlijn, Versie: 3.0. 2014.
18. Mechera R, Schuster T, Rosenberg R, et al. Lymph node yield after rectal resection in patients treated with neoadjuvant radiation for rectal cancer: a systematic review and meta-analysis. *Eur J Cancer*. 2017;72:84–94.
19. Gravante G, Parker R, Elshaer M, et al. Lymph node retrieval for colorectal cancer: estimation of the minimum resection length to achieve at least 12 lymph nodes for the pathological analysis. *Int J Surg*. 2016;25:153–157.
20. Brouwer NPM, Stijns RCH, Lemmens VEPP, et al. Clinical lymph node staging in colorectal cancer; a flip of the coin? *Eur J Surg Oncol*. 2018;44:1241–1246.

21. Markl B, Kerwel TG, Wagner T, et al. Methylene blue injection into the rectal artery as a simple method to improve lymph node harvest in rectal cancer. *Mod Pathol*. 2007;20:797–801.
22. Reima H, Saar H, Innos K, et al. Methylene blue intra-arterial staining of resected colorectal cancer specimens improves accuracy of nodal staging: a randomized controlled trial. *Eur J Surg Oncol*. 2016;42:1642–1646.
23. Markl B, Kerwel TG, Jahnig HG, et al. Methylene blue-assisted lymph node dissection in colon specimens: a prospective, randomized study. *Am J Clin Pathol*. 2008;130:913–919.
24. Borowski DW, Banky B, Banerjee AK, et al. Intra-arterial methylene blue injection into ex vivo colorectal cancer specimens improves lymph node staging accuracy: a randomized controlled trial. *Colorectal Dis*. 2014;16:681–689.
25. Langman G, Patel A, Bowley DM. Size and distribution of lymph nodes in rectal cancer resection specimens. *Dis Colon Rectum*. 2015;58:406–414.
26. Philips BWJ, Fortuin AS, Orzada S, et al. High resolution MR imaging of pelvic lymph nodes at 7 Tesla. *Magn Reson Med*. 2017;78:1020–1028.
27. Marneros AG, Blanco F, Husain S, et al. Classification of cutaneous intravascular breast cancer metastases based on immunolabeling for blood and lymph vessels. *J Am Acad Dermatol*. 2009;60:633–638.
28. Zhang H, Zhang C, Zheng Z, et al. Chemical shift effect predicting lymph node status in rectal cancer using high-resolution MR imaging with node-for-node matched histopathological validation. *Eur Radiol*. 2017;27:3845–3855.
29. Lagemaat MW, Philips BW, Vos EK, et al. Feasibility of multiparametric magnetic resonance imaging of the prostate at 7 T. *Invest Radiol*. 2017;52:295–301.
30. Kerwel TG, Spatz J, Anthuber M, et al. Injecting methylene blue into the inferior mesenteric artery assures an adequate lymph node harvest and eliminates pathologist variability in nodal staging for rectal cancer. *Dis Colon Rectum*. 2009;52:935–941.
31. Tornroos A, Shabo I, Druvefors B, et al. Postoperative intra-arterial methylene blue injection of colorectal cancer specimens increases the number of lymph nodes recovered. *Histopathology*. 2011;58:408–413.
32. Klepsyte E, Samalavicius NE. Injection of methylene blue solution into the inferior mesenteric artery of resected rectal specimens for rectal cancer as a method for increasing the lymph node harvest. *Tech Coloproctol*. 2012;16:207–211.
33. Amajoyi R, Lee Y, Recio PJ, et al. Neoadjuvant therapy for rectal cancer decreases the number of lymph nodes harvested in operative specimens. *Am J Surg*. 2013; 205:289–292; discussion 292.
34. Horne J, Bateman AC, Carr NJ, et al. Lymph node revealing solutions in colorectal cancer: should they be used routinely? *J Clin Pathol*. 2014;67:383–388.
35. Beets-Tan RGH, Lambregts DMJ, Maas M, et al. Magnetic resonance imaging for clinical management of rectal cancer: updated recommendations from the 2016 European Society of Gastrointestinal and Abdominal Radiology (ESGAR) consensus meeting. *Eur Radiol*. 2018;28:1465–1475.
36. Wang C, Zhou Z, Wang Z, et al. Patterns of neoplastic foci and lymph node micrometastasis within the mesorectum. *Langenbecks Arch Surg*. 2005;390:312–318.
37. Märkl B, Rößle J, Arnholdt HM, et al. The clinical significance of lymph node size in colon cancer. *Mod Pathol*. 2012;25:1413–1422.
38. Wang H, Safar B, Wexner S, et al. Lymph node harvest after proctectomy for invasive rectal adenocarcinoma following neoadjuvant therapy: does the same standard apply? *Dis Colon Rectum*. 2009;52:549–557.
39. Bhangu A, Kiran RP, Brown G, et al. Establishing the optimum lymph node yield for diagnosis of stage III rectal cancer. *Tech Coloproctol*. 2014;18:709–717.
40. de la Fuente SG, Manson RJ, Ludwig KA, et al. Neoadjuvant chemoradiation for rectal cancer reduces lymph node harvest in proctectomy specimens. *J Gastrointest Surg*. 2009;13:269–274.
41. Elferink MA, Siesling S, Visser O, et al. Large variation between hospitals and pathology laboratories in lymph node evaluation in colon cancer and its impact on survival, a nationwide population-based study in the Netherlands. *Ann Oncol*. 2011;22:110–117.
42. Evans MD, Barton K, Rees A, et al. The impact of surgeon and pathologist on lymph node retrieval in colorectal cancer and its impact on survival for patients with Dukes' stage B disease. *Colorectal Dis*. 2008;10:157–164.
43. Baxter NN, Virnig DJ, Rothenberger DA, et al. Lymph node evaluation in colorectal cancer patients: a population-based study. *J Natl Cancer Inst*. 2005;97:219–225.
44. Bui L, Rempel E, Reeson D, et al. Lymph node counts, rates of positive lymph nodes, and patient survival for colon cancer surgery in Ontario, Canada: a population-based study. *J Surg Oncol*. 2006;93:439–445.
45. Wright FC, Law CH, Last L, et al. Lymph node retrieval and assessment in stage II colorectal cancer: a population-based study. *Ann Surg Oncol*. 2003;10:903–909.